## PAPER

Check for updates

# Deoxyfluorination tunes the aggregation of cellulose and chitin oligosaccharides and highlights the role of specific hydroxyl groups in the crystallization process†

Giulio Fittolani, [ID] [a,b] Surusch Djalali,[a,b] Manishkumar A. Chaube, [ID] [a]
Theodore Tyrikos-Ergas,‡[a,b] Marlene C. S. Dal Colle,[a,b] Andrea Grafmüller,[c]
Peter H. Seeberger [ID] [a,b] and Martina Delbianco [ID] *[a]

Cellulose and chitin are abundant structural polysaccharides exploited by nature in a large number of applications thanks to their crystallinity. Chemical modifications are commonly employed to tune polysaccharide physical and mechanical properties, but generate heterogeneous mixtures. Thus, the effect of such modifications is not well understood at the molecular level. In this work, we examined how deoxyfluorination (site and pattern) impact the solubility and aggregation of well-defined cellulose and chitin oligomers. While deoxyfluorination increased solubility in water and lowered the crystallinity of cellulose oligomers, chitin was much less affected by the modification. The OH/F substitution also highlighted the role of specific hydroxyl groups in the crystallization process. This work provides guidelines for the design of cellulose- and chitin-based materials. A similar approach can be imagined to prepare cellulose and chitin analogues capable of withstanding enzymatic degradation.

## Introduction

Cellulose[1] and chitin[2] are naturally abundant structural polysaccharides. Plants, fungi, crustaceans, and insects rely on these polysaccharides for generating mechanically stable cell walls and bacteria exploit the fibrous nature of cellulose for creating dense and impenetrable biofilms.[3,4] Cellulose and chitin are based on a similar backbone consisting of β-1,4 linked glucose (Glc) or *N*-acetyl glucosamine (GlcNAc) monosaccharide units, respectively (Fig. 1A). A dense network of inter- and intramolecular hydrogen bonds are responsible for the high crystallinity and insolubility of these two polysaccharides.[5,6] Both polymers share the key intramolecular hydrogen bond between the OH-3 and O-5′ of the following residue. Additionally, cellulose crystal structures display intra-

and inter-molecular hydrogen bond between OH-6′ and OH-2,[5,7,8] while in chitin the NHAc carbonyl group provides further inter-chain stabilization.[6,9,10] Beside hydrogen bonds, additional stabilization is gained from hydrophobic interactions between the C–H rich faces of the monosaccharides.[11]

The crystalline character of cellulose and chitin is key in many applications. For example, cellulose and chitin nanocrystals, CNCs and ChNCs respectively, have raised interest for the fabrication of optical materials.[12–16] While many aspects of cellulose and chitin crystals are established, details on the crystallization process and the precise role of each hydroxyl group is often a matter of debate.[8,9] Furthermore, not all cellulose and chitin allomorphs have yet been described in detail.[17,18] Top-down approaches rely on extraction from natural sources and do not grant access to polysaccharides with uniform dispersity, limiting our understanding of crystallization. Moreover, chemical modification protocols, aiming to tune cellulose and chitin crystallinity, lack control over the modification pattern.[19,20] In contrast, bottom-up approaches guarantee precise saccharide sequences and patterns of modification, important determinants of the materials and biological properties.[21–25]

Perturbing the primary sequence of an oligosaccharide with non-natural residues offers a strategy to systematically tune the macroscopic properties of a material. In addition, this approach provides indirect information on the role of the replaced unit (or functional group). In this regard, fluorination

*[a]Department of Biomolecular Systems, Max Planck Institute of Colloids and Interfaces, Am Mühlenberg 1, 14476 Potsdam, Germany.
E-mail: martina.delbianco@mpikg.mpg.de
[b]Department of Chemistry and Biochemistry, Freie Universität Berlin, Arnimallee 22, 14195 Berlin, Germany
[c]Department of Theory and Biosystems, Max Planck Institute of Colloids and Interfaces, Am Mühlenberg 1, 14476 Potsdam, Germany*
†Electronic supplementary information (ESI) available. See DOI: https://doi.org/10.1039/d2ob01601j
‡Current affiliation: Department of Chemistry, University of Illinois, 61801 Urbana, Illinois, USA.

**8228** | *Org. Biomol. Chem.*, 2022, **20**, 8228–8235

This journal is © The Royal Society of Chemistry 2022

**Fig. 1** (A) Hydrogen bond pattern of cellulose and chitin. (B) Deoxyfluorinated analogues studied in this work. (C) Building blocks used for the AGA of deoxyfluorinated cellulose and chitin backbones.

of monosaccharides has drawn considerable attention.[26] Fluorination is widely explored in medicinal and material chemistry,[27–33] owing to the unique features of the F atom. Fluorine is a small, highly electronegative atom that can replace C–OH, C–H, and C=O bonds with the chemically inert C–F bond.[28,29] Despite the high polarization of the C–F bond, hydrogen bonds involving the fluorine atom are rare. Thus, deoxyfluorination offers a strategy to tune hydrogen bonding and interactions with water molecules with impact on conformation, aggregation propensity, and interactions with proteins.[34,35] To date, most studies are focused on simple monosaccharides;[34,36] limited attention has been given to the construction of more complex fluorinated oligosaccharides which require multistep syntheses, stereo-control, and harsh conditions.[37–39]

Fluorinated cellulose[40] and chitin[41] oligomers, prepared by enzymatic synthesis, suggested that deoxyfluorination affects their crystallinity. Still, enzymatic synthesis does not allow for precise control over the pattern of substitution, degree of polymerization, and have a limited substrate scope.[42] Here, we report the Automated Glycan Assembly (AGA) of a collection of cellulose and chitin oligomers incorporating deoxyfluorinated monosaccharides with precise pattern and site of modification (Fig. 1B and C). Molecular dynamics (MD) simulations served as a tool to interpret and rationalize the systematic characterization of these compounds performed by powder X-ray diffraction (XRD) and NMR spectroscopy. These insights will provide guidance for the future design of cellulose and chitin based materials.

## Results and discussion

### Building blocks synthesis

We targeted the synthesis of deoxyfluorinated cellulose and chitin oligomers as model compounds to understand the role of each hydroxyl group in the crystallization process. We pre-

viously reported that the 3F modification imparts higher flexibility to single cellulose oligomers by disrupting hydrogen bonds and preventing formation of crystalline domains.[22,43] Here, we extend the study to new patterns and site of modification. **BB1–5** were employed to construct the β-1,4 cellulose and chitin backbone using AGA (Fig. 1C). **BB1** and **BB4** were chosen to install the non-modified Glc and GlcNAc units, respectively, while **BB2**, **BB3**, and **BB5** were synthesized to introduce the deoxyfluorinated residues. Each BB was equipped with a reactive anomeric leaving group, either a thioether or a dibutyl phosphate, permanent protecting groups (Bn, Bz, or TCA), and a temporary protecting group (Fmoc) to guarantee the regioselective step-wise elongation of β-1,4 glycosidic linkages. β-Stereoselectivity was ensured by participation of the C-2 Bz or *N*-TCA protecting groups. The synthesis of **BB2** was performed following previously reported procedures.[22] Deoxyfluorinated Glc and GlcNAc BBs (**BB3** and **BB5**) were synthesized from commercially available starting materials, minimizing the number of synthetic steps.

The installation of a fluorine atom at the C-6 position of Glc was envisioned through the regioselective deoxyfluorination of compound **1**, readily accessible in four steps from a commercially available intermediate (see the ESI†). Regioselective tosylation of **1**,[44] followed by the nucleophilic substitution with CsF on intermediate **2**, yielded only trace amounts of desired product **3a** and a significant amount of the elimination side-product **3b** (Fig. 2 and Table S1, entries 1 and 2†). The direct regioselective deoxyfluorination of **1** using DAST in the presence of pyridine resulted in the decomposition of the starting material (Table S1, entries 3 and 4†).[45] When the reaction was performed in the absence of base, compound **3a** was formed as a major product in modest 34% yield (Fig. 2 and Table S1, entries 5 and 6†). Increasing the reaction temperature only led to complex mixtures which complicated isolation (Table S1, entry 7†). The modest yield of the DAST-mediated deoxyfluorination of thioglycoside **1** were ascribed to

This journal is © The Royal Society of Chemistry 2022

*Org. Biomol. Chem.*, 2022, **20**, 8228–8235 | **8229**

Fig. 2   Synthesis of **BB3**.



Fig. 3   Synthesis of **BB5**.

the several side-reactions. Elimination, to give **3b**, is a commonly observed side-reaction in nucleophilic substitution using the basic fluoride ion.[46] A migration of the anomeric SEt moiety[47] can generate **3c** (observed as anomeric fluoride at *ca.* 130–140 ppm in ^{19}F NMR). Lastly, DAST-mediated thioglycoside activation[48–50] can produce reactive species capable of undergoing glycosylation with the nucleophiles present in solution or promote starting material decomposition, as observed when the reaction was performed at higher temperature. After the deoxyfluorination step, installation of Fmoc on **3a** completed the synthesis of **BB3** (Fig. 2).

For the synthesis of the 6F-GlcNAc BB (**BB5**), different deoxyfluorination strategies were explored (Fig. 3). Regioselective deoxyfluorination using DAST on intermediate **4**, bearing three hydroxyl groups, gave a complex mixture of products with only trace amounts of **5** (Fig. 3).[51] Thus, triol **4** was converted into intermediate **6** in two steps, because an efficient deoxyfluorination procedure was reported for an analogous thioglycoside intermediate.[41] The subsequent DAST-mediated deoxyfluorination of **6** yielded a complex mixture of side-products (Fig. 3). Next, inspired by the successful deoxyfluorination of the 3-O-Bn Glc intermediate **1**, triol **4** was converted into diol **9** in three steps (Fig. 3). DAST-mediated deoxyfluorination, performed in a mixture of DCM and 1,4-dioxane, afforded the desired product **10** together with a complex mixture of side-products that complicated purification (Table S1, entry 1†). Furthermore, anomerization[48–50] was observed (Table S2, entry 1†). To simplify purification and characterization, the reaction was performed in ACN as solvent. These conditions yielded the target compound **10** in 23% yield and minimized anomerization[52] (Table S2, entry 2†). To complete the synthesis of **BB5**,
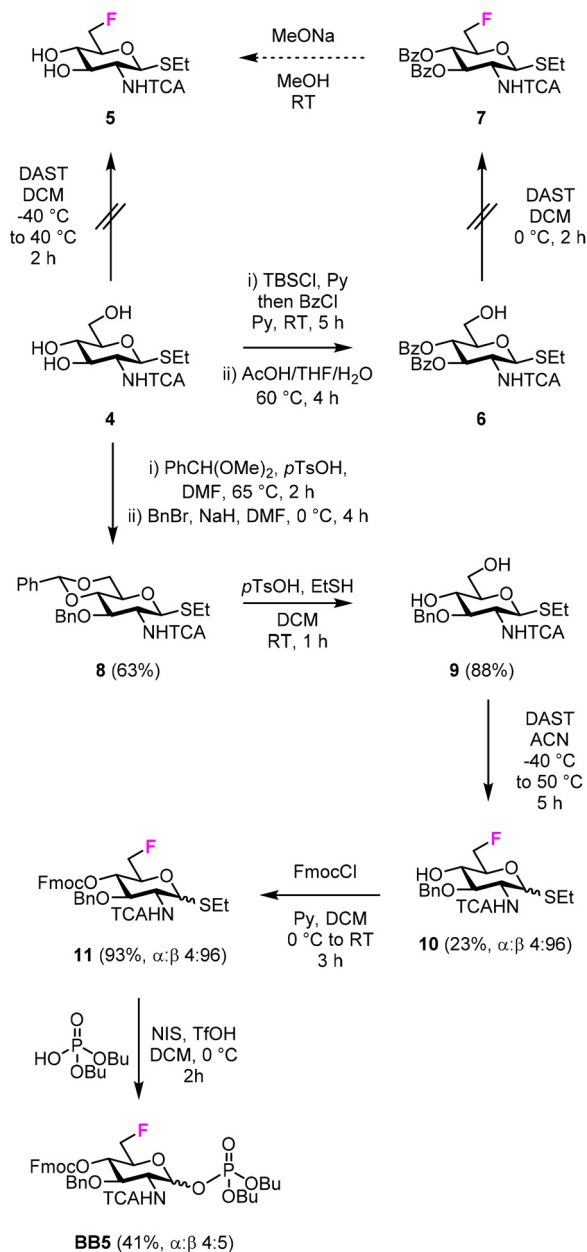
Fmoc was installed and the thioether leaving group replaced by dibutyl phosphate (Fig. 3). The latter step aimed to increase the donor reactivity that could be beneficial when working with unreactive acceptors such as the GlcNAc-OH-4.[52,53] During the installation of the dibutyl phosphate anomeric group, a trichloro oxazoline was also formed[54] (Scheme S1†), but it could be easily converted into the desired **BB5**, adapting a reported procedure.[55]

In both synthetic routes, the success of the C-6 deoxyfluorination of the thioglycoside intermediates proved highly dependent on the protecting group pattern, potentially modulating the rate of the multiple side reactions that can occur.[41,45] While the implementation of a more stable anomeric group

8230 | *Org. Biomol. Chem.*, 2022, **20**, 8228–8235

This journal is © The Royal Society of Chemistry 2022

(*e.g.* O-based glycoside) could overcome the synthetic hurdles associated to the thioether leaving group, this operation would imply additional protecting group manipulations that might result in comparable overall yields. Thus, other routes were not explored.

**Automated glycan assembly of F-cellulose and F-chitin**

Fluorinated cellulose and chitin hexasaccharides were prepared by AGA, following cycles of glycosylation and Fmoc deprotection on solid supports **L1** or **L2** (Fig. 4). Solid-phase methanolysis of Bz esters (Module F, only for cellulose oligomers) was followed by cleavage from the solid support (Module G1) and hydrogenolysis of the Bn and TCA protecting groups (Module H1 or H2). A single final purification step afforded a collection of fluorinated cellulose and chitin oligo-

mers (Module I). For details on the AGA modules we refer to the ESI.†

The cellulose analogues were assembled including either the 3F- or the 6F-Glc units, indicated with a capital **F** and non-capital **f**, respectively. For both analogues, different substitution patterns were explored: alternating (**FAFAFA**), "random" (**AFAAFA** and **AfAAfA**), block (**FFFAAA**, and **fffAAA**), and fully substituted (**FFFFFF** and **ffffff**) (Fig. 4). Two 6F-chitin analogues with "random" (**NNᶠNNNᶠN**) and block (**NᶠNᶠNᶠNNN**) substitution patterns were synthesized (Fig. 4). Deoxyfluorination did not significantly affect the reactivity of the BB donors. The low reactivity of the OH-4[53] of the 6F-GlcNAc acceptors bound to the solid support was circumvented with a double cycle of glycosylation to minimize deletion sequences.



**Fig. 4**  AGA of fluorinated cellulose and chitin oligomers. Yields of isolated products after AGA, deprotection, and purification are reported in parentheses (see the ESI†). The oligomers **A₆**, **N₆**, **AFAAFA** and **FAFAFA** were synthesized according to previously reported protocols.[22] The oligosaccharides are represented following the Symbol Nomenclature For Glycans (SNFG).[56]

This journal is © The Royal Society of Chemistry 2022

*Org. Biomol. Chem.*, 2022, **20**, 8228–8235 | **8231**

## F-cellulose

To analyze the impact of the 3F- and 6F-Glc modifications on the macroscopic properties such as crystallinity, we relied on MD simulations and powder XRD. We previously observed that the 3F-Glc modification disrupted the intramolecular OH-3···O-5′ hydrogen bond in **AFAAFA**, enhancing the flexibility of the single molecule and disrupting the crystallinity typical of cellulose.[22,43] The systematic analysis of all oligomers with different substitution patterns revealed that, while all analogues were more soluble in water (>1 mg mL$^{-1}$) than the unmodified **AAAAAA**, the hexasaccharide with a block pattern (**FFFAAA**) displayed a cellulose II-type XRD profile, despite the high degree of substitution (Fig. 5A). In contrast, when the pattern was alternating (**FAFAFA**) an amorphous XRD profile was obtained. A very different behavior was observed for the hexasaccharide with a block pattern of 6F-Glc residues (**fffAAA**), which displayed again an amorphous XRD. These data indicate that the substitution site (6F *versus* 3F) is a key parameter in the aggregation process (Fig. 5A). This result is consistent with that observed in the Ramachandran plots extracted from single molecule atomistic MD simulations (Fig. 5B); while **FFFAAA** resembled **AAAAAA**, **fffAAA** showed a broader distribution, with a wider range of Ψ dihedral values populated (Fig. 5B, top). The radius of gyration plots confirmed the higher overall single molecule flexibility for the 6F substituted analogue **fffAAA**, exploring extended geometries as well as more compact conformations (Fig. 5B, bottom). This trend was observed for all the 3F and 6F analogues (see ESI, Section 4.3†). At high degree of substitution, both 3F and 6F oligomers resulted in amorphous XRDs (Fig. 5A).

The introduction of fluorine into the oligosaccharides enabled the use of the $^{19}$F NMR channel to perform structural studies.[34,57] The $^{19}$F NMR spectrum of **FFFAAA** in deuterium oxide (D$_2$O) indicated a different chemical environment surrounding the 3F moiety (*i.e.* internal *versus* external units, *ca.* 2.5 ppm difference), potentially due to significantly different interactions with solvent molecules (Fig. 6A). In contrast, **fffAAA** displayed a smaller chemical shift difference between internal and external residues (*ca.* 1 ppm, Fig. 6C). For the 6F substituted analogues, $^{19}$F NMR allowed for a qualitative analysis[58] of the populations of the ω dihedral angle, using the calculated values for the three ω rotamers as reference[59,60] (Fig. 6B). We measured the $^{3}J_{H5-F6}$ values for external (27.2 Hz) and internal (25.8 Hz) residues (Fig. 6C), suggesting a lower populated gg rotamer in the external residue compared to internal ones. A complete estimation of the gg, gt, and tg populations required an additional experimental value (*i.e.* $^{3}J_{H6-H5}$) which could not be extracted due to severe spectral overlap in the $^{1}$H NMR. MD simulations supported this experimental observation, showing a similar trend of less populated gg conformations for external residues, both for **AAAAAA** (Fig. 6D, top) and for **fffAAA** (Fig. 6D, bottom). Furthermore, fluorine at the C-6 showed across all simulated structures a small rise of the tg rotamer (see the ESI, Section 4.6†), that could not be detected by NMR. This is surprising because the electronegative fluorine substituent should favor the gg rotamer due to the *gauche* effect.[61] We speculate that these populations could be the results of the fluorine atom disrupting the organization of the surrounding water molecules[62] (see the ESI†) or an artifact of the force field.

Overall, these data suggest that the 6F substitution has a bigger impact than the 3F substitution on the crystallization of cellulose oligomers. This implies that the OH-6 plays a more important role than OH-3 in the crystallization process, potentially due to its higher exposure to solvent molecules, as indicated by NMR analysis of the 3F and 6F analogues. The higher exposure to water also suggest the prominent role of OH-6 in the formation of intermolecular hydrogen bonds, triggering aggregation.



**Fig. 5** (A) Powder XRD profiles of 3F- and 6F-cellulose compared to cellulose II profile (dotted line). (B) Ramachandran plots for all glycosidic linkages combined (top) and radius of gyration plots (bottom) extracted from the MD simulations. The dihedral angles are defined as Φ = H1C1O4C4 and Ψ = C1O4C4H4 (further details are reported in Fig. S3 in the ESI†).

8232 | *Org. Biomol. Chem.*, 2022, **20**, 8228–8235

This journal is © The Royal Society of Chemistry 2022

**Fig. 6** (A) Fluorinated cellobiose repeating unit (top) and excerpt of the $^{19}$F NMR of **FFFAAA** in D$_2$O (bottom). (B) Definition of gg, gt, and tg rotamers of the ω dihedral angle and previously reported calculated $^3J_{H5-F6}$ values.[59,60] (C) Excerpt of the $^{19}$F NMR of **fffAAA** in D$_2$O and respective $^3J_{H5-F6}$ values. (D) Predicted populations of the rotamers for the ω dihedral angles for external (left) and internal (right) residues of two cellulose analogues.



**Fig. 7** (A) Powder XRD profiles of 6F-chitin compared to α-chitin profile (dotted line). (B) Ramachandran plots for all glycosidic linkages combined (top) and radius of gyration plots (bottom) extracted from the MD simulations.

### F-chitin

In contrast to 6F-cellulose, the two 6F-chitin oligomers with 'random' (**NN$^f$NNN$^f$N**) and block (**N$^f$N$^f$N$^f$NNN**) pattern were less soluble in water (<2 mg mL$^{-1}$) than **NNNNNN** (13–17 mg mL$^{-1}$ (ref. 22)). Both analogues retained the α-chitin-type XRD profile and the conformational behavior observed for the natural counterpart (**NNNNNN**)[22] (Fig. 7A). High similarity in the Ramachandran and radius of gyration plots indicated comparable molecular conformations, with tendency to adopt an extended shape (Fig. 7B). We qualitatively analyzed the ω dihedral angle by measuring the $^3J_{H5-F6}$ coupling constants for **N$^f$N$^f$N$^f$NNN**. The smaller $^3J_{H5-F6}$ for external residues was interpreted as a less populated gg rotamer compared to internal ones, as observed for the 6F-cellulose analogues (Fig. S6A and S6B†).

From these results, it appears that chitin is more tolerant than cellulose to C-6 modifications, supporting the hypothesis that chitin crystallization is driven by other functionalities (e.g.

the amide group that stabilizes inter-sheet hydrogen bonds[10]) rather than the OH-6. In the crystal structure of α-chitin the C-6 side chain can adopt a variety of orientations,[6,10] supporting the observed high tolerance of chitin for C-6 modifications.

## Conclusions

Seven new fluorinated oligomers of cellulose and chitin were assembled by AGA using non-natural 3F-Glc, 6F-Glc and 6F-GlcNAc BBs, granting precise control over the oligomer length and fluorination pattern. Their conformational behavior and macroscopic properties were studied by XRD analysis, NMR spectroscopy, and MD simulations. While, in general, deoxyfluorination of cellulose results in higher water solubility and lower crystallinity, we found that the pattern (block versus alternated) and site of modification (3F versus 6F) can be

This journal is © The Royal Society of Chemistry 2022

Org. Biomol. Chem., 2022, **20**, 8228–8235 | **8233**

exploited to tune the sample crystallinity. In cellulose, the 6F modification impacted the molecular conformation more than the 3F substitution. In contrast, chitin conformation was much less affected by the 6F modification, with all the F-chitin retaining the native crystallinity.

This work highlights deoxyfluorination as a valuable mean to tune the solubility and aggregation of cellulose and chitin as well as to pinpoint the importance of the replaced hydroxyl group in the crystallization process. In the future, deoxyfluorination can be imagined to increase the stability towards enzymatic degradation of cellulose or chitin-based materials.

## Conflicts of interest

The authors declare no competing financial interest.

## Acknowledgements

## References

1  Y. Nishiyama, *J. Wood Sci.*, 2009, **55**, 241–249.
2  M. Rinaudo, *Prog. Polym. Sci.*, 2006, **31**, 603–632.
3  D. J. Cosgrove, *Nat. Rev. Mol. Cell Biol.*, 2005, **6**, 850–861.
4  H.-C. Flemming, J. Wingender, U. Szewzyk, P. Steinberg, S. A. Rice and S. Kjelleberg, *Nat. Rev. Microbiol.*, 2016, **14**, 563–575.
5  Y. Nishiyama, J. Sugiyama, H. Chanzy and P. Langan, *J. Am. Chem. Soc.*, 2003, **125**, 14300–14306.
6  P. Sikorski, R. Hori and M. Wada, *Biomacromolecules*, 2009, **10**, 1100–1105.
7  P. Langan, Y. Nishiyama and H. Chanzy, *Biomacromolecules*, 2001, **2**, 410–416.
8  P. Chen, Y. Ogawa, Y. Nishiyama, M. Bergenstråhle-Wohlert and K. Mazeau, *Cellulose*, 2015, **22**, 1485–1493.
9  Y. Ogawa, C. M. Lee, Y. Nishiyama and S. H. Kim, *Macromolecules*, 2016, **49**, 7025–7031.
10 R. Minke and J. Blackwell, *J. Mol. Biol.*, 1978, **120**, 167–181.
11 B. Medronho, A. Romano, M. G. Miguel, L. Stigsson and B. Lindman, *Cellulose*, 2012, **19**, 581–587.
12 B. Frka-Petesic and S. Vignolini, *Nat. Photonics*, 2019, **13**, 365–367.
13 R. M. Parker, G. Guidetti, C. A. Williams, T. Zhao, A. Narkevicius, S. Vignolini and B. Frka-Petesic, *Adv. Mater.*, 2018, **30**, 1704477.
14 R. M. Parker, B. Frka-Petesic, G. Guidetti, G. Kamita, G. Consani, C. Abell and S. Vignolini, *ACS Nano*, 2016, **10**, 8443–8449.
15 A. Narkevicius, L. M. Steiner, R. M. Parker, Y. Ogawa, B. Frka-Petesic and S. Vignolini, *Biomacromolecules*, 2019, **20**, 2830–2838.
16 A. Narkevicius, R. M. Parker, J. Ferrer-Orri, T. G. Parton, Z. Lu, G. T. Kerkhof, B. Frka-Petesic and S. Vignolini, *Adv. Mater.*, 2022, 2203300.
17 M. Wada, L. Heux and J. Sugiyama, *Biomacromolecules*, 2004, **5**, 1385–1391.
18 Y. Ogawa, J.-L. Putaux and Y. Nishiyama, *Curr. Opin. Chem. Biol.*, 2022, **70**, 102183.
19 S. C. Fox, B. Li, D. Xu and K. J. Edgar, *Biomacromolecules*, 2011, **12**, 1956–1972.
20 H. C. Arca, L. I. Mosquera-Giraldo, V. Bi, D. Xu, L. S. Taylor and K. J. Edgar, *Biomacromolecules*, 2018, **19**, 2351–2376.
21 G. Fittolani, D. Vargová, P. H. Seeberger, Y. Ogawa and M. Delbianco, *J. Am. Chem. Soc.*, 2022, **144**, 12469–12475.
22 Y. Yu, T. Tyrikos-Ergas, Y. Zhu, G. Fittolani, V. Bordoni, A. Singhal, R. J. Fair, A. Grafmüller, P. H. Seeberger and M. Delbianco, *Angew. Chem., Int. Ed.*, 2019, **58**, 13127–13132.
23 T. Tyrikos-Ergas, V. Bordoni, G. Fittolani, M. A. Chaube, A. Grafmüller, P. H. Seeberger and M. Delbianco, *Chem. – Eur. J.*, 2021, **27**, 2321–2325.
24 S. Basa, M. Nampally, T. Honorato, S. N. Das, A. R. Podile, N. E. El Gueddari and B. M. Moerschbacher, *J. Am. Chem. Soc.*, 2020, **142**, 1975–1986.
25 T. Tyrikos-Ergas, S. Gim, J. Huang, S. Pinzón Martín, D. Varón Silva, P. H. Seeberger and M. Delbianco, *Nat. Commun.*, 2022, **13**, 3954.
26 K. Huonnic and B. Linclau, *Chem. Rev.*, DOI: **10.1021/acs.chemrev.2c00086**.
27 S. Purser, P. R. Moore, S. Swallow and V. Gouverneur, *Chem. Soc. Rev.*, 2008, **37**, 320–330.
28 J. C. Biffinger, H. W. Kim and S. G. DiMagno, *ChemBioChem*, 2004, **5**, 622–627.
29 D. O'hagan, *Chem. Soc. Rev.*, 2008, **37**, 308–319.
30 E. P. Gillis, K. J. Eastman, M. D. Hill, D. J. Donnelly and N. A. Meanwell, *J. Med. Chem.*, 2015, **58**, 8315–8359.
31 R. Hevey, *Chem. – Eur. J.*, 2021, **27**, 2240–2253.
32 N. A. Meanwell, *J. Med. Chem.*, 2018, **61**, 5822–5880.
33 M. Inoue, Y. Sumii and N. Shibata, *ACS Omega*, 2020, **5**, 10633–10640.
34 B. Linclau, A. Ardá, N.-C. Reichardt, M. Sollogoub, L. Unione, S. P. Vincent and J. Jiménez-Barbero, *Chem. Soc. Rev.*, 2020, **49**, 3863–3888.
35 J. D. Martínez, A. I. Manzano, E. Calviño, A. De Diego, B. Rodriguez de Francisco, C. Romanò, S. Oscarson, O. Millet, H.-J. Gabius, J. Jiménez-Barbero and F. J. Cañada, *J. Org. Chem.*, 2020, **85**, 16072–16081.
36 V. Denavit, J. St-Gelais, T. Tremblay and D. Giguére, *Chem. – Eur. J.*, 2019, 201901346.
37 M. L. Uhrig, B. Lantaño and A. Postigo, *Org. Biomol. Chem.*, 2019, **17**, 5173–5189.

**8234** | *Org. Biomol. Chem.*, 2022, **20**, 8228–8235

This journal is © The Royal Society of Chemistry 2022

38 T. J. Kieser, N. Santschi, L. Nowack, A. Axer, G. Kehr, S. Albrecht and R. Gilmour, *ACS Chem. Neurosci.*, 2020, **11**, 2129–2136.

39 A. Axer, R. P. Jumde, S. Adam, A. Faust, M. Schäfers, M. Fobker, J. Koehnke, A. K. H. Hirsch and R. Gilmour, *Chem. Sci.*, 2021, **12**, 1286–1294.

40 P. Andrade, J. C. Muñoz-García, G. Pergolizzi, V. Gabrielli, S. A. Nepogodiev, D. Iuga, L. Fábián, R. Nigmatullin, M. A. Johns, R. Harniman, S. J. Eichhorn, J. Angulo, Y. Z. Khimyak and R. A. Field, *Chem. – Eur. J.*, 2021, **27**, 1374–1382.

41 A. Makino, M. Ohmae and S. Kobayashi, *Macromol. Biosci.*, 2006, **6**, 862–872.

42 T. Keenan, F. Parmeggiani, J. Malassis, C. Q. Fontenelle, J.-B. Vendeville, W. Offen, P. Both, K. Huang, A. Marchesi, A. Heyam, C. Young, S. J. Charnock, G. J. Davies, B. Linclau, S. L. Flitsch and M. A. Fascione, *Cell Chem. Biol.*, 2020, **27**, 1199–1206.

43 K. Anggara, Y. Zhu, G. Fittolani, Y. Yu, T. Tyrikos-Ergas, M. Delbianco, S. Rauschenbach, S. Abb, P. H. Seeberger and K. Kern, *Proc. Natl. Acad. Sci. U. S. A.*, 2021, **118**, 1–6.

44 Y. Zhu, T. Tyrikos-Ergas, K. Schiefelbein, A. Grafmüller, P. H. Seeberger and M. Delbianco, *Org. Biomol. Chem.*, 2020, **18**, 1349–1353.

45 D. A. Williams, K. Pradhan, A. Paul, I. R. Olin, O. T. Tuck, K. D. Moulton, S. S. Kulkarni and D. H. Dube, *Chem. Sci.*, 2020, **11**, 1761–1774.

46 P. A. Champagne, J. Desroches, J. D. Hamel, M. Vandamme and J. F. Paquin, *Chem. Rev.*, 2015, **115**, 9073–9174.

47 P.-C. Lin, A. K. Adak, S.-H. Ueng, L.-D. Huang, K.-T. Huang, J. A. Ho and C.-C. Lin, *J. Org. Chem.*, 2009, **74**, 4041–4048.

48 K. C. Nicolaou, R. E. Dolle and D. P. Papahatjis, *J. Am. Chem. Soc.*, 1984, **106**, 4189–4192.

49 K. Suzuki, Y. Ito and O. Kanie, *Carbohydr. Res.*, 2012, **359**, 81–91.

50 I. Ohtsuka, T. Ako, R. Kato, S. Daikoku, S. Koroghi, T. Kanemitsu and O. Kanie, *Carbohydr. Res.*, 2006, **341**, 1476–1487.

51 P. J. Card and G. S. Reddy, *J. Org. Chem.*, 1983, **48**, 4734–4743.

52 P. R. Andreana and D. Crich, *ACS Cent. Sci.*, 2021, **7**, 1454–1462.

53 D. Crich and V. Dudkin, *J. Am. Chem. Soc.*, 2001, **123**, 6819–6825.

54 R. Enugala, L. C. R. Carvalho, M. J. Dias Pires and M. M. B. Marques, *Chem. – Asian J.*, 2012, **7**, 2482–2501.

55 T. J. Donohoe, J. G. Logan and D. D. P. Laffan, *Org. Lett.*, 2003, **5**, 4995–4998.

56 A. Varki, R. D. Cummings, M. Aebi, N. H. Packer, P. H. Seeberger, J. D. Esko, P. Stanley, G. Hart, A. Darvill, T. Kinoshita, J. J. Prestegard, R. L. Schnaar, H. H. Freeze, J. D. Marth, C. R. Bertozzi, M. E. Etzler, M. Frank, J. F. Vliegenthart, T. Lütteke, S. Perez, E. Bolton, P. Rudd, J. Paulson, M. Kanehisa, P. Toukach, K. F. Aoki-Kinoshita, A. Dell, H. Narimatsu, W. York, N. Taniguchi and S. Kornfeld, *Glycobiology*, 2015, **25**, 1323–1324.

57 P. Valverde, J. I. Quintana, J. I. Santos, A. Ardá and J. Jiménez-Barbero, *ACS Omega*, 2019, **4**, 13618–13630.

58 V. Denavit, D. Lainé, C. Bouzriba, E. Shanina, É. Gillon, S. Fortin, C. Rademacher, A. Imberty and D. Giguère, *Chem. – Eur. J.*, 2019, **25**, 4478–4490.

59 R. J. Abraham, E. J. Chambers and W. A. Thomas, *Magn. Reson. Chem.*, 1992, **30**, S60–S65.

60 L. Phillips and V. Wray, *J. Chem. Soc. B*, 1971, 1618.

61 N. Santschi, N. Aiguabella, V. Lewe and R. Gilmour, *J. Fluor. Chem.*, 2015, **179**, 96–101.

62 R. E. Rosenberg, *J. Phys. Chem. A*, 2019, **123**, 7651–7660.

This journal is © The Royal Society of Chemistry 2022

*Org. Biomol. Chem.*, 2022, **20**, 8228–8235 | **8235**